



## RESEARCH ARTICLE

10.1029/2019MS001750

## Toward an Energetically Consistent, Resolution Aware Parameterization of Ocean Mesoscale Eddies

Malte F. Jansen<sup>1</sup> , Alistair Adcroft<sup>2,3</sup> , Sina Khani<sup>1,2</sup> , and Hailu Kong<sup>1</sup> <sup>1</sup>Department of the Geophysical Sciences, The University of Chicago, Chicago, IL, USA, <sup>2</sup>Atmospheric and Oceanic Sciences, Princeton University, Princeton, NJ, USA, <sup>3</sup>NOAA Geophysical Fluid Dynamics Laboratory, Princeton, NJ, USA

## Key Points:

- A scale-aware energy budget-based eddy parameterization is introduced
- Bidirectional energy transfer between resolved flow and subgrid scales can be represented
- The parameterization allows for a smooth transition between non-eddy and eddy resolution regimes

## Correspondence to:

M. F. Jansen,  
mfj@uchicago.edu

## Citation:

Jansen, M. F., Adcroft, A., Khani, S., & Kong, H. (2019). Toward an energetically consistent, resolution aware parameterization of ocean mesoscale eddies. *Journal of Advances in Modeling Earth Systems*, 11, 2844–2860. <https://doi.org/10.1029/2019MS001750>

Received 22 MAY 2019

Accepted 2 AUG 2019

Accepted article online 7 AUG 2019

Published online 28 AUG 2019

**Abstract** A subgrid-scale eddy parameterization is developed, which makes use of an explicit eddy kinetic energy budget and can be applied at both “non-eddy” and “eddy-permitting” resolutions. The subgrid-scale eddies exchange energy with the resolved flow in both directions via a parameterization of baroclinic instability (based on the established formulation of Gent and McWilliams) and biharmonic and negative Laplacian viscosity terms. This formulation represents the turbulent cascades of energy and enstrophy consistent with our current understanding of the turbulent eddy energy cycle. At the same time, the approach is simple and general enough to be readily implemented in ocean climate models, without adding significant computational cost. The closure has been implemented in the Modular Ocean Model Version 6 and tested in the “Neverworld” configuration, which employs an idealized analytically defined topography designed as a testbed for mesoscale eddy parameterizations. The parameterization performs well over a range of resolutions, seamlessly connecting non-eddy and eddy-resolving regimes.

## 1. Introduction

Most of the kinetic energy (KE) in the ocean is in the form of mesoscale (O(10–100) km) eddies (e.g., Ferrari & Wunsch, 2009), which play a crucial role in the transport of heat, salt, and biogeochemical tracers, both directly via stirring and mixing and indirectly via their effect on the large-scale ocean circulation (e.g., Busecke et al., 2014; Gill et al., 1974; Gnanadesikan et al., 2015; Hallberg & Gnanadesikan, 2006; Johnson & Bryden, 1989; McWilliams, 2008; Waterman et al., 2011). Since mesoscale ocean eddies are relatively small, it is inherently challenging to represent their effects in global ocean and climate models. Many global ocean and climate models today have insufficient resolution to resolve any significant mesoscale eddy activity and their effect needs to be entirely parameterized (e.g., Meijers, 2014). An increasing number of global models meanwhile are entering the so-called “eddy-permitting” resolution regime (grid spacing  $\lesssim (1/4)^\circ$ ), where the largest mesoscale features can be resolved explicitly (e.g., Griffies et al., 2015; Kuhlbrodt et al., 2015; Menemenlis et al., 2008). However, due to the wide range of scales and scale interactions in ocean turbulence, eddy-permitting models still rely heavily on adequate parameterizations of subgrid-scale eddy effects (e.g., Fox-Kemper & Menemenlis, 2008; Jansen et al., 2015; Roberts & Marshall, 1998).

To identify the processes that need to be represented by a subgrid eddy parameterization at different resolutions, we can build on our understanding of the energetics of mesoscale eddies. According to the theory of quasi-geostrophic (QG) turbulence (Jansen & Held, 2014; Larichev & Held, 1995; Rhines, 1979; Salmon, 1980; Vallis, 2006), the largest eddies extract available potential energy (APE) from the mean flow by perturbing the large-scale mean density gradient, thus converting mean into eddy APE. Eddy APE is then transferred to smaller scales before being converted into eddy kinetic energy (EKE) near the scale of the deformation radius. Finally, EKE is transferred to larger scales until the inverse cascade is halted by friction or a turbulence-wave transition. At scales smaller than the deformation radius, enstrophy (i.e., vorticity variance), but no energy, is cascaded toward small scales. Energy fluxes in the real ocean are likely to be significantly more complex than this idealized picture, primarily due to interactions with topography and the potential for loss of balance, which can trigger a forward energy cascade. Moreover, the idealized picture sketched above assumes a large scale separation between the mean flow and the eddies and again between the largest eddies and the deformation radius. Clear scale separations are, however, not usually found in Earth's ocean. Nevertheless, we expect the idealized QG theory to provide a useful guide as to what processes are likely to be important at different scales (e.g., Arbic et al., 2013; Ferrari & Wunsch, 2009; Scott & Wang, 2005; von Storch et al., 2012).

©2019. The Authors.

This is an open access article under the terms of the Creative Commons Attribution License, which permits use, distribution and reproduction in any medium, provided the original work is properly cited.

In cognizance of the increasing resolution of global models, there has recently been a push toward the development of improved parameterizations for ocean models in the so-called eddy-permitting resolution regime, where the largest eddies are at least marginally resolved (Bachman et al., 2017; Griffies & Hallberg, 2000; Fox-Kemper & Menemenlis, 2008; Hallberg, 2013; Jansen & Held, 2014; Jansen et al., 2015; Mana & Zanna, 2014; Zanna et al., 2017). Jansen and Held (2014) and Jansen et al. (2015) developed a new parameterization for subgrid-scale eddy momentum fluxes in eddy-permitting models based on our physical understanding of energy and enstrophy cascades in geostrophic turbulence. Noting the need to remove enstrophy at the grid scale without spuriously dissipating KE, a biharmonic viscosity operator was combined with a negative Laplacian viscosity to represent the backscatter of KE to the resolved flow. The magnitude of the backscatter is regulated via an explicit subgrid KE budget, which closes the energy budget and stabilizes the parameterization despite the presence of a negative viscosity. The energy budget-based backscatter parameterization has so far been tested in a number of idealized configurations, including baroclinic channel flows (Jansen & Held, 2014; Jansen et al., 2015; Juricke et al., 2019) and a barotropic gyre model (Klöwer et al., 2018), where it substantially improves the solutions at resolutions where the largest eddies are at least marginally resolved. Unfortunately, even so-called eddy-permitting global ocean and climate models today reach this resolution only over part of the world's ocean while remaining non-eddying in other regions (e.g., Hallberg, 2013). Moreover, coarser resolution ocean models remain the workhorse for long-term climate simulations, thus limiting the usefulness of a subgrid-scale parameterization that remains inadequate in the non-eddying regime.

Energy budget-based mesoscale eddy parameterizations have also been proposed for the non-eddying resolution regime (Cessi, 2008; Eden & Greatbatch, 2008; Jansen et al., 2015; Mak et al., 2018; Marshall & Adcroft, 2010). Rather than addressing the parameterization of momentum and associated KE and enstrophy fluxes, these studies focus on eddy volume fluxes (or “bolus” transport), parameterized via a variant of the Gent and McWilliams (1990, GM) parameterization, which removes APE from the resolved flow by flattening isopycnal slopes. Eden and Greatbatch (2008) introduce an explicit subgrid mesoscale EKE budget equation where the potential energy dissipation from the resolved flow by the GM parameterization appears as a source of subgrid EKE. The predicted EKE then informs the GM coefficient, which is formulated via a mixing length argument. A variant of this approach has more recently been proposed by Mak et al. (2017, 2018), who formulate the GM coefficient via an energetic constraint, which provides a strict upper bound in the QG limit. Energy budget-based GM closures have shown promise in non-eddying ocean models (Eden & Greatbatch, 2008; Mak et al., 2017, 2018), but their success hinges on an adequate representation of the mixing length and eddy energy dissipation (Jansen et al., 2015), both of which remain highly challenging to predict from first principles. Moreover, these approaches fundamentally remain variations on the GM closure, merely providing a flow-dependent GM coefficient. While suitable for non-eddying models, the GM parameterization has been argued to be too dissipative at eddy-permitting resolution, where its main effect is to dampen potentially resolvable eddies (Hallberg, 2013).

The challenge to eddy parameterizations in the eddy-permitting regime can be understood by noting their effect on the energy cycle. The GM parameterization dissipates APE at the grid scale and can hence be thought of as representing the forward cascade of APE and ultimately conversion to subgrid-scale EKE. The viscous frictional operator parameterizes a forward cascade of enstrophy but also spuriously dissipates a significant amount of KE (e.g., Jansen & Held, 2014). A pathway for KE to return to the resolved flow instead is generally missing in global ocean models. The KE backscatter term introduced by Jansen and Held (2014) attempts to account for this issue but by focusing on KE and enstrophy fluxes only, the parameterization is unsuitable if the conversion of APE to KE near the deformation scale cannot be resolved explicitly.

To allow for a complete representation of the turbulent eddy energy cycle at different scales, we here propose a generalized energy budget-based eddy parameterization, which combines the backscatter approach of Jansen et al. (2015) with an energy budget-based version of the GM parameterization following Eden and Greatbatch (2008) and others (e.g., Jansen et al., 2015; Marshall & Adcroft, 2010). The resulting closure can represent forward and inverse cascades of KE (realized via viscous friction and backscatter operators), as well as the conversion of potential to KE at the subgrid scale (via the GM parameterization). An adequate representation of these processes is paramount to making the approach applicable over a wide range of resolutions and parameter regimes—a crucial step for global ocean and climate models, where flow properties vary widely across the domain. A related approach has independently been developed by Bachman (2019)

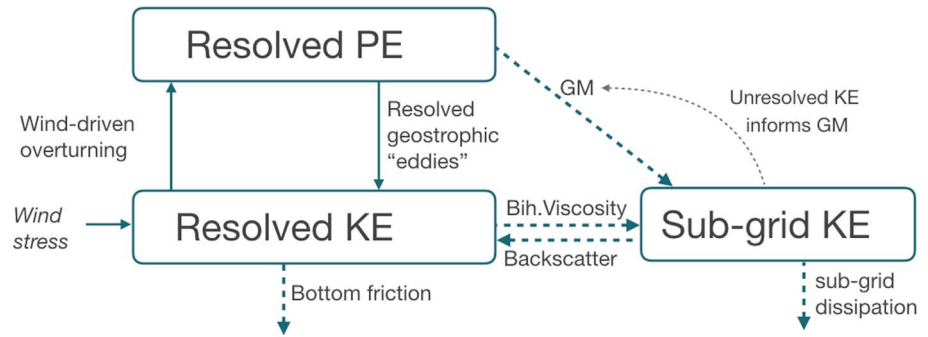


**Figure 1.** Sketch of the model's energy cycle, indicating transfers between PE, resolved KE, and unresolved (subgrid-scale) KE. Explicitly resolved energy transfers are denoted by solid arrows, while parameterized transfers are denoted by dashed arrows. Notice that diapycnal mixing provides an additional source of PE in the ocean (e.g., Wunsch & Ferrari, 2004) but is not included here, as we will focus on adiabatic dynamics. Similarly, a decomposition of potential energy into available and background PE is not attempted. Such a decomposition is generally nontrivial in primitive equations and not necessary for the present purpose, as total and available PE tendencies are interchangeable for adiabatic dynamics. KE = kinetic energy; GM = Gent and McWilliams; PE = potential energy.

and tested successfully in an Eady channel model. Similarities and differences between our parameterization and the formulation of Bachman (2019) will be discussed in section 5.

The parameterization has been implemented in the latest version of the Modular Ocean Model Version 6 (MOM6) and is tested in the idealized “Neverworld” ocean configuration, which includes an analytically defined topography with two basins and a circumpolar channel. The specifics of the new parameterization will be discussed in section 2. The model setup and fine-resolution reference simulations will be presented in section 3, and results will be discussed in section 4. Conclusions are provided in section 5.

## 2. A Scale-Aware Energy Budget-Based Eddy Parameterization

This study introduces an energy budget-based subgrid-scale eddy parameterization framework for ocean general circulation models that is suitable over a wide range of resolutions from non-eddy to eddy resolving. The parameterization is motivated by our physical understanding of the ocean's turbulent energy cycle and makes use of an explicit subgrid EKE equation:

$$\partial_t e = \dot{e}_{GM} + \dot{e}_{v_4} - \dot{e}_{v_2} - \dot{e}_{diss} - \frac{1}{H} \nabla \cdot (H \mathbf{F}_b), \quad (1)$$

where  $e$  is the vertically averaged subgrid KE. A GM parameterization extracts potential energy from the resolved flow, which appears as a source of subgrid KE ( $\dot{e}_{GM}$ ). Another source of subgrid KE is given by a biharmonic viscosity ( $\dot{e}_{v_4}$ ), which extracts KE and enstrophy from the resolved flow. Sinks of subgrid KE include a subgrid-scale dissipation ( $\dot{e}_{diss}$ ), as well as a backscatter of KE to the resolved flow ( $\dot{e}_{v_2}$ ), implemented via a negative Laplacian viscosity. The last term in equation (1) represents horizontal transport of subgrid KE. The major energy pathways, represented by the different components of the parameterization, and the major (potentially) resolved pathways are sketched in Figure 1. Notice that the computational overhead associated with the vertically averaged subgrid energy budget is small as it amounts to a single two-dimensional tracer.

The GM parameterization is formulated to address three distinct resolution regimes. One where none of the mesoscale eddies are resolvable, one where the largest eddies can be resolved explicitly, but the deformation radius remains unresolved, and one where the deformation radius is resolved. In the real ocean, the scale of the largest eddies is only modestly larger than the deformation radius (perhaps by about a factor of 2—see e.g., Tulloch et al., 2011), such that the second regime may be hard to separate from the others. Nevertheless, both theory and observations suggest that the scale of the largest eddies is controlled by an arrest scale that generally differs from the deformation radius (e.g., Larichev & Held, 1995; Tulloch et al., 2011), which encourages us to treat the two scales as independent. With that in mind, we propose a formulation for the GM “diffusivity” as follows:

$$K_{GM} = c\sqrt{2e}L_{mix}R(\Delta k_d). \quad (2)$$

Here  $c$  is a nondimensional parameter, which will be used to tune the parameterization,  $L_{\text{mix}}$  is a subgrid-scale mixing length, and  $R(\Delta k_d)$  is a resolution function to account for the lack of a forward cascade of APE below the deformation radius.  $\Delta$  is the grid spacing, and  $k_d$  is the deformation wavenumber, calculated by solving an eigenvalue problem for the first vertical mode (e.g., Flierl, 1978). We here focus only on the leading vertical mode, thus ignoring transfer of energy into higher modes (see also Appendix A).

The subgrid-scale mixing length is defined to be the smaller of the grid scale and a halting scale:

$$L_{\text{mix}} = \min(\Delta, L_{\beta^*}), \quad (3)$$

where the halting scale is assumed to be given by a generalized Rhines scale

$$L_{\beta^*} = (2e)^{1/4} \beta^{*-1/2}, \quad (4)$$

with a topographically modified barotropic planetary potential vorticity gradient  $\beta^* = |\beta \hat{y} - f \nabla H / H|$ , where  $\beta = \partial_y f$  is the planetary vorticity gradient and  $H$  is the local depth of the ocean (see also Sinha & Richards, 1999; Thompson, 2010). The use of a topographic Rhines scale was found to provide better results at coarse resolution than a traditional definition of the Rhines scale (not shown). A GM coefficient similar to the formulation of Mak et al. (2018) could be implemented via a mixing length that is proportional to  $\sqrt{e} N / M^2$ , where  $N^2 = \partial_z^2 b$  and  $M^2 = |\nabla_h b|$  (cf. Jansen et al., 2015). Such a formulation may provide a useful upper bound on the GM coefficient, although the results of Jansen et al. (2015) suggest that the Rhines scale is likely to limit the mixing length over most of the relevant parameter regime. For simplicity, an additional limitation of the GM coefficient following Mak et al. (2018) is therefore not included here.

The nondimensional resolution function

$$R(\Delta k_d) = \left[ 1 + \frac{\pi}{\Delta k_d} \right]^{-1} \quad (5)$$

further reduces the GM diffusivity once the deformation wavelength is resolved. Since we do not expect the forward cascade of APE to continue at scales smaller than the deformation radius (e.g., Larichev & Held, 1995), the GM parameterization becomes obsolete at high enough resolutions. The scaling of  $R(\Delta k_d) \propto \Delta$  for  $\Delta^{-1} \gg k_d$  can be crudely justified in the context of two-layer QG theory (see Appendix A) and appears to provide reasonably good results in practice. A resolution function to scale the GM coefficient as a function of  $\Delta k_d$  has previously been introduced by Hallberg (2013), who advocates for a step function dependence, where the GM parameterization is suddenly switched off once  $\Delta k_d$  falls below a threshold value. The argument is that any intermediate value for the GM coefficient primarily leads to a damping of the eddies that may otherwise be resolvable while not doing enough to parameterize the missing eddy transport. We hypothesize that this problem can be avoided with the inclusion of KE backscatter, which counteracts the damping of resolvable eddies by the GM parameterization, thus allowing for a smooth transition between non-eddy and eddy-resolving regimes.

The energy transfer between the resolved flow and subgrid KE associated with the GM parameterization is formulated as

$$\dot{e}_{\text{GM}} = \frac{1}{H} \sum_k K_{\text{GM}} g'_k |\nabla_\sigma \eta_k|^2, \quad (6)$$

where we assume a stacked shallow water model, as used in this study, and the sum is over all isopycnal layer interfaces,  $k$ , with height  $\eta_k$  and reduced gravity  $g'_k$ . According to the QG energy cycle, potential energy extracted from the large-scale flow by mesoscale eddies is converted first into eddy APE, with the final conversion to eddy KE being generally delayed (Chen et al., 2016). One could account for this pathway by including an additional explicit subgrid APE budget. However, the formulation of the GM parameterization, at least in  $z$  coordinate models, is arguably inconsistent with such an approach, as the eddy buoyancy flux is generally assumed to be directed locally along isopycnals, which implies a direct and complete conversion of all eddy APE into eddy KE (Chen et al., 2014; Lorenz, 1955). Moreover, formalizing the concept of APE and its transfers outside the QG limit is challenging. For simplicity and consistency, we therefore ignore the subgrid APE reservoir for the time being, although we note that the topic deserves further attention in the future.

The biharmonic viscosity is formulated similar to the OM4 global ocean model configuration of MOM6, which combines a biharmonic version of the Smagorinsky model (Griffies & Hallberg, 2000; Smagorinsky, 1963) with a resolution-dependent background viscosity:

$$\nu_4 = (c_{\text{smag}}|D| + \tau_{\text{vis}}^{-1})\Delta^4, \quad (7)$$

where  $|D| = \sqrt{(\partial_x u - \partial_y v)^2 + (\partial_y u + \partial_x v)^2}$  is the deformation rate,  $c_{\text{smag}} = 0.06$ , and  $\tau_{\text{vis}} = 45$  days. The only difference to the OM4 configuration is in the use of a fixed time scale rather than a fixed velocity scale in the formulation of the background viscosity, which we believe to lead to a more realistic resolution dependence. (In a forward enstrophy cascade —or, more generally, in the presence of a  $k^{-3}$  KE spectrum —we expect the grid-scale eddy turnover time scale rather than the grid-scale eddy velocity to be scale independent). The dissipation time scale  $\tau_{\text{vis}}$  is chosen to provide about the same biharmonic background viscosity as in the OM4 configuration at  $(1/2)^\circ$  resolution.

The corresponding energy transfer between the resolved and unresolved flow can be computed as

$$\dot{e}_{\nu_4} = -\frac{1}{H} \int \tau_{ij}^{\nu_4} \partial_i u_j dz, \quad (8)$$

where  $\tau^{\nu_4}$  is the biharmonic stress tensor (Griffies & Hallberg, 2000),  $i, j = x, y$  represent the horizontal directions and, following Einstein notation, sums over recurring indices are implied.

In an effort to minimize the number of free parameters (and for lack of a better theory), the negative viscosity coefficient in the parameterization of KE backscatter is chosen to be identical to the GM coefficient, that is,  $\nu_2 = -K_{\text{GM}}$ . This formulation has the desirable property that in a limit where the dominant balance is between the forward cascade of APE and the inverse cascade of KE (an informative limit in QG theory, albeit unlikely to ever hold in the real ocean), the closure will lead to an approximate equipartition between grid-scale APE and KE. The approximate equipartitioning follows by noting that a similar energy flux requires that  $-\int \tau_{ij}^{\nu_2} \partial_i u_j dz = \sum_k K_{\text{GM}} g'_k |\nabla_\sigma \eta_k|^2$ . Assuming that both shear and isopycnal height gradients are dominated by grid-scale variability (as expected in APE and KE cascade ranges), we can further use that  $\int \tau_{ij}^{\nu_2} \partial_i u_j dz \sim H \nu_2 \Delta^{-2} KE_\Delta$  and  $\sum_k K_{\text{GM}} g'_k |\nabla_\sigma \eta_k|^2 \sim H K_{\text{GM}} \Delta^{-2} APE_\Delta$ , where  $KE_\Delta$  and  $APE_\Delta$  are the characteristic grid-scale KE and APE, respectively. If  $K_{\text{GM}} = -\nu_2$ , we hence find  $KE_\Delta \approx APE_\Delta$ . The approach also has the effect that both GM and backscatter are expected to become negligible at very fine resolution, leaving only the biharmonic Smagorinsky closure at work. Whether the backscatter term should become small at fine resolution remains an open question. We tried an alternative formulation where the resolution function,  $R(\Delta k_d)$ , is not included in the backscatter term, in which case the closure effectively reduces to that of Jansen et al. (2015) at fine resolution. The results compared less favorably to our reference simulation, with the combined resolved and parameterized eddy fluxes apparently becoming too strong at relatively fine resolutions (not shown). The energy transfer associated with the backscatter ( $\dot{e}_{\nu_2}$ ) is analogous to equation (8) but with the negative Laplacian stress tensor replacing the biharmonic tensor (see Griffies & Hallberg, 2000, for the formulation of the stress tensors).

The subgrid-scale KE dissipation is assumed to be dominated by frictional dissipation in the bottom boundary layer. The latter is parameterized using a quadratic drag law as

$$\dot{e}_{\text{diss}} = c_d \sqrt{(e + \mathbf{u}_{\text{bot}}^2 + U_{\text{bg}}^2)} e, \quad (9)$$

where  $c_d = 0.03$  is the drag coefficient,  $\mathbf{u}_{\text{bot}}$  is the resolved bottom velocity, and  $U_{\text{bg}} = 0.1$  m/s is a background velocity representing tidal currents and other unresolved (non-mesoscale) flows. The formulation in (9) implicitly assumes that the subgrid KE is dominated by the barotropic mode, such that the KE at the bottom is similar to the vertically averaged KE represented by  $e$ . This assumption is likely to lead to an overestimate of the bottom velocity and hence dissipation (e.g., Jansen et al., 2015). At the same time, we are missing other potential dissipation processes, such as associated with energy transfer to the internal wave field and other routes to loss of balance (e.g., Ferrari & Wunsch, 2009; Wunsch & Ferrari, 2004). In practice, the formulation in equation (9) appears to provide roughly the right level of subgrid EKE in our model, although the success may in part be due to unrealistically strong bottom friction compensating for other missing processes. More research is needed to better understand the routes to dissipation of mesoscale energy in the ocean (Wunsch & Ferrari, 2004; Ferrari & Wunsch, 2009).

The last term in the subgrid KE budget equation (1) represents the horizontal transport of subgrid KE, which is here parameterized via diffusion and advection by the resolved barotropic flow (cf. Grooms, 2017):

$$\mathbf{F}_e = \mathbf{u}_{\text{bt}} e - K_e \nabla e, \quad (10)$$

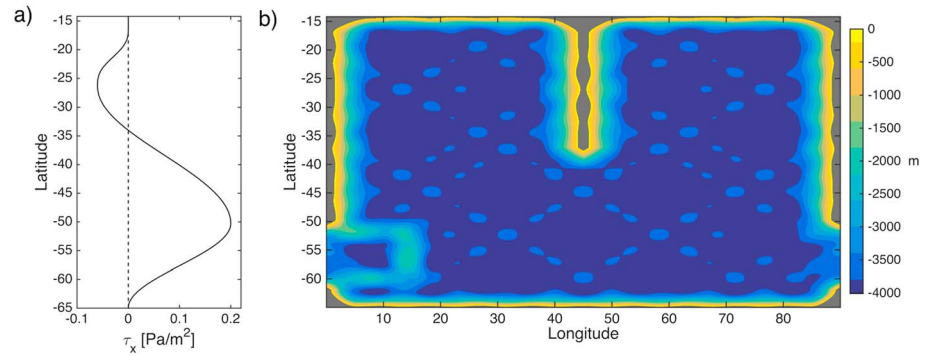


**Figure 2.** Zonal wind stress (a) and bathymetry (b) of the Neverworld configuration. No meridional wind stress is applied. The bottom topography in the interior of the basins extends up to 400 m above the seafloor, which otherwise is at 4-km depth. Gray shading indicates land.

where  $\mathbf{u}_{bt}$  is the resolved barotropic (i.e., vertical mean) velocity and  $K_e$  is a diffusivity of subgrid KE. Notice that horizontal boundaries in our model are implemented via vanishing ocean thickness,  $H$ , and the formulation of the flux term in equation (1) implies no flux boundary conditions for eddy energy. The subgrid KE diffusivity is chosen as  $K_e = c\sqrt{2e}L_{mix}$ . In lack of a better theory, the nondimensional parameter  $c$  is again chosen identical to that in the GM parameterization. In addition to being advected by the large-scale flow and stirred by the turbulent velocity field itself, we expect an eddy energy flux due to Rossby wave-like propagation (e.g., Zhai et al., 2010). This process is not currently included in our model but could be added given a suitable theory for wave-like eddy energy propagation. Grooms (2017) moreover shows that, while the mean propagation of eddy energy may be reasonably represented by a Laplacian diffusion, instantaneous eddy energy distributions are poorly represented by the mean, suggesting that a stochastic representation of subgrid EKE transport may be a promising avenue for future improvements.

In addition to explicit parameterizations, numerical methods can play a significant role in the energy and enstrophy budget at eddy-permitting resolutions. We here use a discretization of the momentum equations based on Arakawa and Hsu (1990), which exactly conserves energy and enstrophy in the limit of horizontally nondivergent flow. An exception is the  $(1/16)^\circ$  reference simulation, which had already been performed using the enstrophy conserving scheme of Sadourny (1975).

### 3. Model and Test Setup

The parameterization introduced in section 2 has been implemented in the Geophysical Fluid Dynamics Laboratory (GFDL) MOM6 and will here be tested in the Neverworld configuration. The Neverworld configuration, which has been designed specifically as a testbed for mesoscale eddy parameterizations, uses an idealized Southern-Hemisphere-like bathymetry and zonal wind stress (see Figure 2). The domain, which extends from  $14^\circ\text{S}$  to  $65^\circ\text{S}$  and over  $90^\circ$  zonally, comprises two basins connected to a circumpolar ocean region in the south. Below about 2-km depth, the circumpolar channel is interrupted by topography mimicking Scotia Arc, and smaller seafloor undulations (extending up to 400m above this maximum depth) exist throughout the domain. A flow is forced by a zonally symmetric zonal wind stress with westerlies south of  $\sim 33^\circ\text{S}$  and weaker easterlies to the north. The topography and forcing are analytically defined, which allows us to readily run simulations at arbitrary resolutions. The model setup uses six isopycnal vertical layers with  $\rho = 1025.5, 1027, 1027.5, 1027.8, 1028,$  and  $1028.1 \text{ kg/m}^3$  from top to bottom, respectively. All layer interfaces are initially flat with layer thicknesses of 150, 250, 600, 1000, 1000, and 1000 m, respectively. The adiabatic setup allows us to integrate the model to a statistically steady state, which is reached after less than 100 model years. The time step is set to 300 s for the finest resolution simulation at  $(1/16)^\circ$  and is increased inversely proportional to the grid spacing (up to a maximum of 1 hr) for the coarser resolution simulations.

A fine-resolution reference simulation has been performed on a Mercator grid with  $(1/16)^\circ$  nominal resolution and will serve as a “ground truth” for the evaluation of our eddy parameterization in coarser-resolution simulations. The reference simulation uses a biharmonic viscosity but no GM parameterization, as the con-

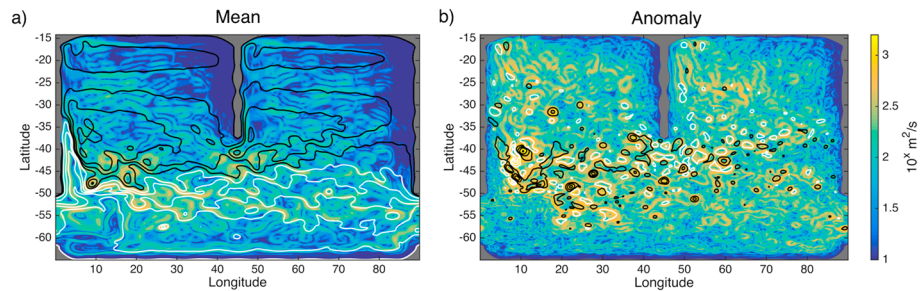


**Figure 3.** Mean flow and eddies in the fine-resolution ( $(1/16)^\circ$ ) reference simulation. (a) Time-mean sea surface height, with black contours indicating positive values and white contours indicating negative values, and magnitude of the vertically integrated transport (shading; with logarithmic color bar). Averages are taken over the last 20 years of the 100-year-long simulation. (b) As in (a) but showing a snapshot of deviations from the time mean. The sea surface height contour interval is 0.2 m in (a) and 0.4 m in (b).

version of potential to KE near the deformation radius is expected to be adequately resolved. Figure 3 shows the time-mean horizontal flow and a snapshot of the eddy field in the fine-resolution reference simulation. The flow shows many of the familiar features observed in the real ocean. A circumpolar current develops, which is associated with a strong transient eddy field as well as standing meanders—most notably a sharp recirculation downstream of “Drake Passage.” Both basins exhibit gyres, which are partially connected through the Southern Ocean. Energetic transient eddies exist throughout the domain and are most pronounced downstream of Drake Passage, as well as near the tip of the central continent, where coherent vortices, crudely resembling Aghulas rings, are formed. The KE spectrum indicates that the most energetic eddies have a wavelength of around  $3\text{--}4^\circ$  longitude, corresponding to around 200–400 km (see Figure 4).

The new parameterization discussed in section 2 (hereafter: MEKE GM+BS—Mesoscale Eddy Kinetic Energy budget-based GM with BackScatter) will be tested in the Neverworld configuration and compared to other parameterizations available in the MOM6 ocean model. Our primary point of comparison will be the parameterization currently used in GFDL’s OM4p5 ocean-ice model. The OM4p5 global ocean model makes use of an explicit subgrid eddy energy budget similar to equation (1). However, the parameterization employed in OM4p5 differs from the approach presented in section 2 in two main aspects: (1) It does not include energy backscatter to the resolved flow and (2) the resolution dependence of the GM diffusivity is implemented via a step function, following Hallberg (2013). Specifically, the GM coefficient is formulated as in equation (2) but with  $L_{\text{mix}}$  independent of resolution and  $R(\Delta k_d)$  implemented as a step function,

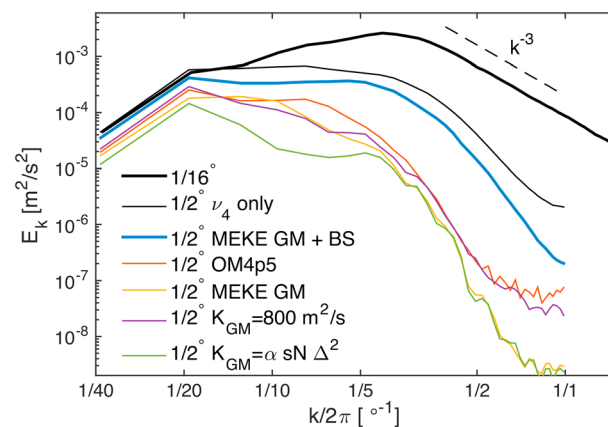


**Figure 4.** Surface geostrophic kinetic energy spectra for the  $(1/16)^\circ$  reference simulation (thick black line) and for  $(1/2)^\circ$  resolution experiments using different formulations for the parameterization of unresolved mesoscale eddy fluxes (see legend and text for explanation). The spectra show geostrophic kinetic energy (computed from sea surface height) of the meridional (transverse) flow as a function of zonal wavenumber. Zonal spectra are taken in both basins between  $3.6^\circ$  and  $41.4^\circ$  and between  $48.6^\circ$  and  $86.4^\circ$  longitude, with tapering applied via a Hann window. Spectra are averaged between both regions, meridionally between  $-62^\circ$  and  $-18^\circ$  latitude, and temporally over the last 20 years of the simulations, and normalized such that a sum over all wavenumbers yields the total energy.

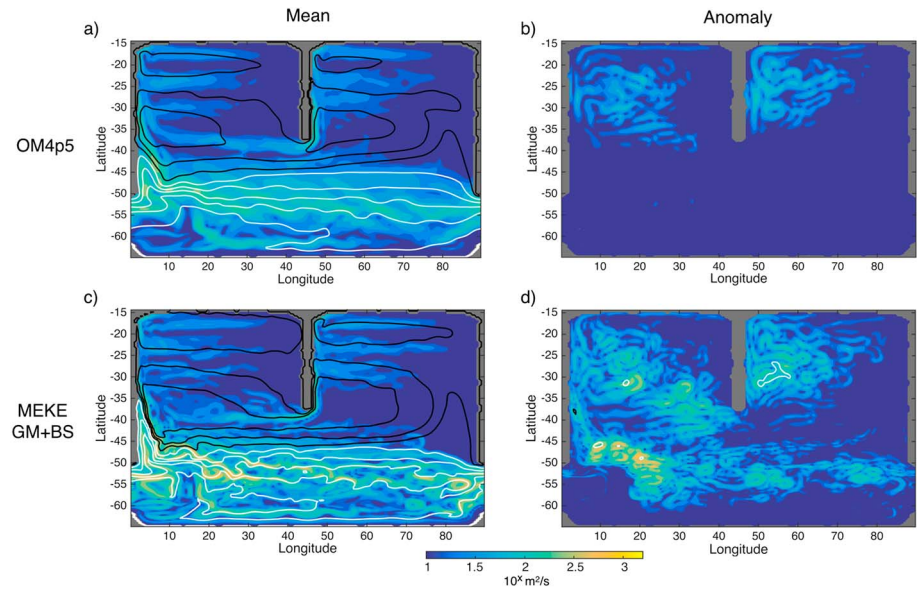


**Figure 5.** As Figure 3 but for  $(1/2)^\circ$  resolution simulations using the parameterization employed in Geophysical Fluid Dynamics Laboratory’s OM4p5 (a and b) versus the new MEKE GM+BS parameterization (c and d).

which turns off the GM parameterization whenever the grid scale is finer than the deformation radius. The OM4p5 parameterization also includes a vertical structure for the GM coefficient (although the subgrid KE budget remains two-dimensional), as well as a Laplacian viscosity. Moreover, the viscous energy dissipation does not affect the subgrid KE. Further details are provided in Appendix B. In addition to the parameterization used in OM4p5, we will consider three different formulations of the GM parameterization, as well as a series of simulations that use only a biharmonic viscosity. The GM formulations include (1) an energy budget-based GM parameterization identical to the configuration discussed in section 2 but without KE backscatter or a subgrid KE source from viscous stress, that is,  $\dot{e}_{v_4} = \dot{e}_{v_2} = 0$  (hereafter: MEKE GM), (2) a constant GM coefficient, and (3) a resolution-dependent variation on the Visbeck et al. (1997) parameterization, with  $K_{GM} = \alpha[sN]\Delta^2$ , where  $s$  is the isopycnal slope,  $N = \sqrt{\partial_z b}$  is the buoyancy frequency,  $\alpha$  is a nondimensional parameter, and the square brackets denote a vertical average. All configurations use the same formulation for the biharmonic viscosity, following equation (7).

In all cases, the parameterizations have been tuned at  $(1/2)^\circ$  resolution to match the mean state APE of the fine-resolution reference solution. The mean state APE is computed as

$$APE = \frac{1}{2} \sum_{i,j,k} A_{i,j} g'_k (\bar{\eta}_{i,j,k}^2 - \tilde{\eta}_{i,j,k}^2), \quad (11)$$

where  $A_{i,j}$  is the area of the grid box at horizontal index  $(i,j)$ ,  $g'_k$  is the reduced gravity of the  $k$ th interface,  $\bar{\eta}_{i,j,k}$  is the time-averaged interface height, and  $\tilde{\eta}_{i,j,k}$  is the interface height of the reference state (defined as the minimum potential energy state that can be obtained via an adiabatic rearrangement of water masses). Since our model setup is adiabatic, the reference state  $\tilde{\eta}$  is constant in time and fully determined by the initial conditions. As a result, total PE and APE differ only by a constant offset and can be used interchangeably. Since mesoscale eddies (as well as parameterizations representing their effects) extract APE from the mean flow, the mean state APE provides a useful metric for the average magnitude of (parameterized and/or resolved) mesoscale eddy effects. Notice that APE is computed on the respective native model grid for both fine- and coarse-resolution simulations. Coarse graining of the fine-resolution simulation results by box averaging over the coarse grid box size has no significant effect, since APE is dominated by the large scales (cf. Figure A1). In all configurations (except the series of simulations without any GM parameterization) one tunable parameter has been adjusted to match the mean state APE. For the energy budget-based parameterizations, which include the new MEKE GM+BS parameterization, the MEKE GM configuration (without backscatter), and the OM4p5 parameterization, the tunable parameter is the nondimensional constant “ $c$ ” in the definition of the GM diffusivity

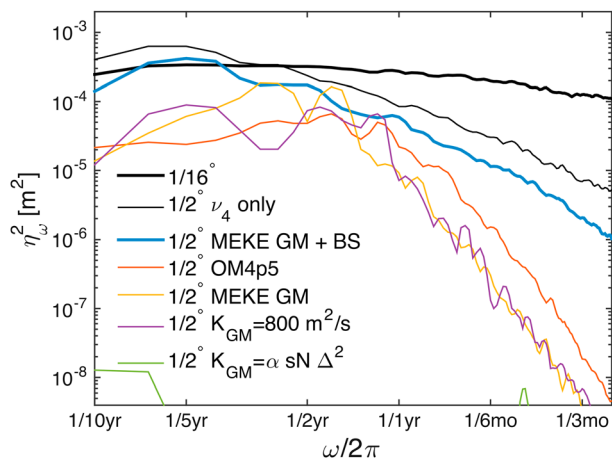


**Figure 6.** Spectra of temporal sea surface height variance (averaged over the model domain) for the fine-resolution reference simulation (thick black line) and  $(1/2)^\circ$  resolution simulations with different subgrid-scale eddy parameterizations (see legend and text for explanation). Notice that the resolution-dependent Visbeck et al. (1997) parameterization (green) leads to a virtually steady solution, such that the variability spectrum is mostly below the axis limit. All spectra have been smoothed with a three point running mean.

(equation (2)). The parameter was determined to be  $c = 0.15$  for MEKE GM+BS,  $c = 0.6$  for MEKE GM, and  $c = 0.115$  for the OM4p5 parameterization. For the constant GM coefficient, the tunable parameter is the diffusivity itself, whose ideal value was found to be  $K_{GM} = 800 \text{ m}^2/\text{s}$ , and for the resolution-dependent formulation of the Visbeck et al. (1997) parameterization the tunable parameter is  $\alpha$ , which was set to  $\alpha=1.1$ . (Notice that this value is much larger than the value of  $\alpha = 0.015$  suggested by Visbeck et al., 1997. The difference is that the original formulation of Visbeck et al., 1997, uses a length scale characteristic of the width of the baroclinic zone [following Green, 1970], while the length scale is here replaced with the [much smaller] grid scale—motivated by the notion that only those eddies that cannot be resolved explicitly need to be parameterized.) Parameters have only been tuned once for the  $(1/2)^\circ$  resolution simulations. Any resolution dependence is determined by the parameterization itself. Notice that all formulations, except for the constant GM parameterization, are resolution dependent, although the explicit resolution dependence is locally binary in the OM4p5 formulation—that is, the GM parameterization is either fully on or off (following the recommendation of Hallberg, 2013).

#### 4. Results

Coarse-resolution simulations with parameterized subgrid-scale eddies have been performed at  $1^\circ$ ,  $(2/3)^\circ$ ,  $(1/2)^\circ$ ,  $(1/3)^\circ$ ,  $(1/4)^\circ$ , and  $(1/6)^\circ$  resolu-

tion. We will start with a discussion of the model results at  $(1/2)^\circ$  resolution, before turning our attention toward resolution dependence.

##### 4.1. $(1/2)^\circ$ Resolution Simulations

At a grid scale of  $(1/2)^\circ$ , adequate resolution of the full mesoscale eddy field is not possible, but the largest transient eddies and most of the standing meanders are resolvable (see also Figures 3 and 4). In practice, the use of the GM parameterization, however, typically leads to a smooth solution with almost no transient eddy activity, as shown for the OM4p5 parameterization configuration in Figures 5a and 5b. Some

transient variability exists in the northern gyre, but the Antarctic Circumpolar Current (ACC) is essentially steady. The time-mean flow is also much smoother than in the fine-resolution reference simulation (cf. Figure 5a to Figure 3a). The new MEKE GM+BS parameterization with KE backscatter, by comparison, leads to a significantly more energetic flow, with a much sharper recirculation in the lee of Drake Passage and transient eddy activity throughout most of the domain (Figures 5c and 5d). Figure 4 confirms quantitatively that the KE at all scales is significantly larger with the MEKE GM+BS parameterization as compared to any of the other  $(1/2)^\circ$  resolution simulations with GM parameterization. However, for all but the largest scales, the KE remains significantly smaller than in the fine-resolution reference simulation and slightly smaller than in a  $(1/2)^\circ$  resolution simulation with no GM parameterization and only hyperviscosity. Higher KE could be obtained by using a stronger backscatter and/or smaller GM coefficient, although preliminary experiments have shown that this tends to lead to a less accurate reproduction of the mean state of the fine-resolution simulation (not shown). Similarly, using only hyperviscosity leads to a poor representation of the mean state, as will be discussed below.

The increased eddy energy in the simulation with energetically consistent backscatter also leads to improved internal variability. Figure 6 shows the sea surface height frequency spectrum of both the fine-resolution reference simulation and the  $(1/2)^\circ$  resolution simulations. While all  $(1/2)^\circ$  resolution simulations have significantly reduced variability on short

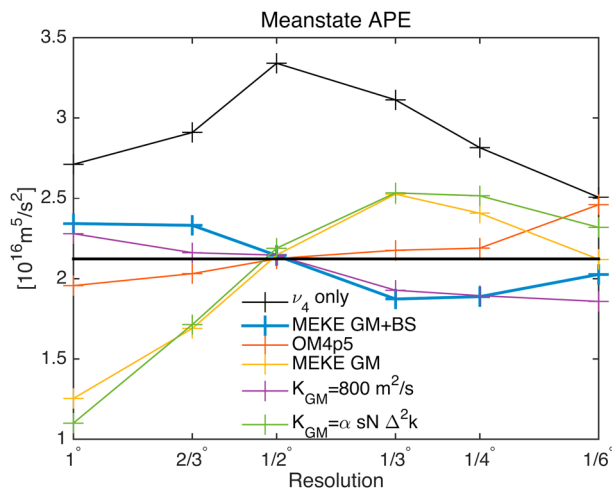


**Figure 7.** Mean state APE as a function of resolution, using different parameterization schemes (see legend). The thick black horizontal line shows the mean state Available potential energy (APE) of the fine-resolution reference simulation. Notice that the mean state APE at  $(1/2)^\circ$  resolution was used to tune the GM parameterizations.

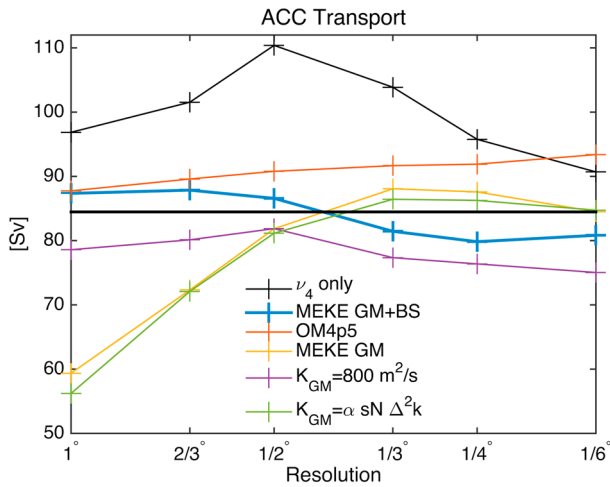


**Figure 8.** ACC transport as a function of resolution, using different parameterization schemes (see legend). The thick black horizontal line shows the ACC transport in the fine-resolution reference simulation.

remains insufficient to adequately resolve mesoscale eddies explicitly. The simulations using the new MEKE GM+BS parameterization show somewhat too high mean state APE at resolutions coarser than  $(1/2)^\circ$  and somewhat too low APE at resolutions finer than  $(1/2)^\circ$ . However, the APE remains within about 10% of the fine-resolution reference simulation throughout the full range of resolutions. Similarly small errors are found using the OM4p5 parameterization configuration, as well as with a constant GM coefficient. The MEKE GM parameterization without backscatter and the resolution-dependent Visbeck et al. (1997) parameterization instead lead to substantially too little APE at resolutions coarser than  $(1/2)^\circ$  and too much APE at resolutions finer than  $(1/2)^\circ$ , indicating that the resolution dependence is inadequate. The relatively poor performance of the MEKE GM and resolution-dependent Visbeck et al. (1997) parameterizations, compared to a constant GM coefficient, is qualitatively consistent with the results of Hallberg (2013), who argued that the GM parameterization should either be fully on or fully off, as a reduced GM coefficient at intermediate resolutions generates too little transport while damping the otherwise resolvable eddies. However, our results also suggest that this problem can be overcome by including a backscatter term, which returns KE to the resolved flow, thereby counteracting the damping of the resolvable eddies by the GM parameterization. Indeed, the largely opposite resolution dependence of the mean state APE in the MEKE GM versus MEKE GM+BS parameterization indicates that the backscatter may somewhat overcompensate in our implementation.

While the mean state APE provides a useful measure of the bulk eddy effect, a correct APE does not guarantee an accurate representation of the mean flow. To quantify the skill of the parameterizations in representing the mean flow across resolutions, we consider two additional metrics: the ACC transport and the global mean isopycnal interface height error. The ACC transport is computed as the total zonal volume transport:

$$T_{ACC} = \iint \bar{u} dx dz, \quad (12)$$

where  $\bar{u}$  is the time-mean zonal flow and the integral extends vertically and meridionally across the full domain. Notice that due to continuity,  $T_{ACC}$  is independent of the longitude where it is evaluated. The mean isopycnal interface height error is computed as

$$\epsilon = \sum_{i,j,k} A_{i,j} g'_k [\bar{\eta}_{i,j,k} - \bar{\eta}_k^{\text{ref}}(\mathbf{x}_{i,j})]^2 / \sum_{i,j} A_{i,j}, \quad (13)$$

where  $\bar{\eta}_k^{\text{ref}}(\mathbf{x}_{i,j})$  is the time-mean interface height of the fine-resolution reference simulation, evaluated at the location of the respective coarse-resolution grid point. Notice that  $\epsilon$  has the dimensions of APE per unit area, but unlike a vanishing error in the mean state APE,  $\epsilon = 0$  would imply a perfect representation of the

time scales as compared to the fine-resolution reference simulation, the new MEKE GM+BS parameterization leads to significantly stronger variability than found with any of the other GM parameterizations and matches the variability of the fine-resolution simulation on interannual time scales. Notice that coarse-graining the fine-resolution reference simulation to a  $(1/2)^\circ$  grid by box averaging does not significantly affect the frequency spectrum (not shown), suggesting that the mismatch between coarse- and fine-resolution simulations is indeed indicative of a model bias.

#### 4.2. Resolution Dependence

To analyze the skill of the parameterization across varying resolution, we first focus on the APE of the mean flow, as defined in equation (11), which provides a useful measure of the overall effectiveness of resolved and parameterized mesoscale eddies. Figure 7 shows the mean state APE as a function of resolution from  $1^\circ$  to  $(1/6)^\circ$ . The mean state APE at  $(1/2)^\circ$  resolution was used to tune the parameterizations and thus by construction matches the APE of the fine-resolution reference simulation in all configurations that use a GM parameterization. No tuning was performed for the simulation that uses only hyperviscosity, where the mean state APE is much too large. Insufficient APE dissipation is expected in this simulation as no GM parameterization is employed and the resolution

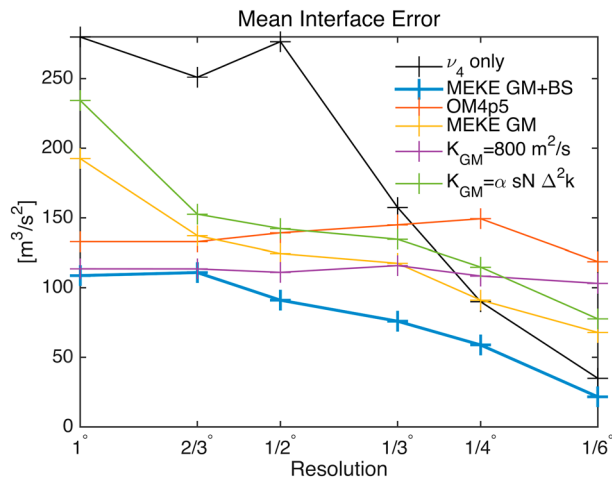


**Figure 9.** Mean isopycnal interface height error, as defined in equation (13), as a function of resolution, using different parameterization schemes (see legend).

(to a lesser extent) OM4p5 parameterizations perform reasonably well at coarse resolution, but the results do not improve systematically as the resolution is increased. The lack of improvement with increasing resolution when using a constant GM coefficient can be understood by noting that the GM parameterization suppresses smaller-scale variability and maintains smooth solutions, thus limiting the effective resolution of the model. The results obtained with the OM4p5 configuration can be understood similarly, as the GM coefficient here remains effectively resolution independent over most of the domain for resolutions up to  $(1/4)^\circ$ . Only at  $(1/6)^\circ$  resolution does the deformation radius become resolved over a large part of the domain where the GM parameterization gets turned off. At resolutions finer than  $(1/4)^\circ$ , relatively good results can also be obtained without a GM parameterization, but this approach leads to a poor representation of the mean state at coarser resolution.

To better understand the representation of eddies at varying resolution, Figure 10 shows the resolved and subgrid KE as a function of model resolution. The subgrid KE is predicted by the parameterization and is defined only for the energy budget-based parameterizations.

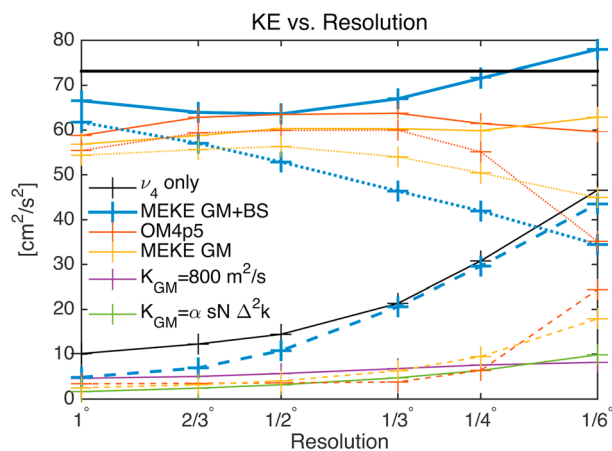


**Figure 10.** Resolved (dashed), subgrid (dotted), and total (solid) kinetic energy (KE) as a function of resolution, using different parameterization schemes (see legend). Notice that subgrid KE is only defined for the energy budget-based parameterizations.

time-mean isopycnal and free surface height fields (and hence also the geostrophic velocity field). A vanishing isopycnal height error would thus also imply that the APE exactly matches the high-resolution reference simulation, but not vice versa.

The results for the ACC transport largely resemble those for the mean state APE (cf. Figure 8 to Figure 7). A close relationship between APE and ACC transport is to be expected as the ACC transport is mostly baroclinic and the associated isopycnal slopes are a major contributor to the APE of our Southern Hemisphere domain. The most notable difference between the results for APE and ACC transport is that the constant GM parameterization leads to a slight but systematic underestimate of the ACC transport, while the OM4p5 configuration leads to a systematic overestimate of the ACC transport. These errors are likely attributable to shortcomings in the spatial patterns of the diffusivity in the two parameterizations. The MEKE GM+BS parameterization instead leads to the overall best agreement with the fine-resolution reference simulation, with an error of less than 10% across the full range of resolutions.

The MEKE GM+BS parameterization also leads to the smallest isopycnal interface height errors, as well as a mean state that systematically improves with increasing resolution (see Figure 9). The constant GM and (to a lesser extent) OM4p5 parameterizations perform reasonably well at coarse resolution, but the results do not improve systematically as the resolution is increased. The lack of improvement with increasing resolution when using a constant GM coefficient can be understood by noting that the GM parameterization suppresses smaller-scale variability and maintains smooth solutions, thus limiting the effective resolution of the model. The results obtained with the OM4p5 configuration can be understood similarly, as the GM coefficient here remains effectively resolution independent over most of the domain for resolutions up to  $(1/4)^\circ$ . Only at  $(1/6)^\circ$  resolution does the deformation radius become resolved over a large part of the domain where the GM parameterization gets turned off. At resolutions finer than  $(1/4)^\circ$ , relatively good results can also be obtained without a GM parameterization, but this approach leads to a poor representation of the mean state at coarser resolution.

In the simulations using the MEKE GM+BS parameterization, the total KE, defined as the sum of the resolved and subgrid KE, roughly matches the total KE of the fine-resolution simulation (to within <15%) across the full range of resolutions. At coarse resolution that KE is almost entirely unresolved, but as the resolution is enhanced, an increasing fraction of the KE is represented by the resolved flow, with the resolved KE starting to dominate at  $(1/6)^\circ$  resolution. A qualitatively similar result is obtained with the MEKE GM and OM4p5 energy budget-based parameterizations, but the fraction of KE that is resolved explicitly remains much smaller throughout the considered range of resolutions. At resolutions of  $(1/3)^\circ$  or finer, the resolved KE of the simulations with the new MEKE GM+BS parameterization is roughly similar to that in the simulations with only hyperviscosity. All other GM-based approaches instead lead to much less energetic flows.

The increasingly resolved KE in the MEKE GM+BS parameterization goes together with changes in the energy budget of the resolved flow (Figure 11). At coarse resolution, the energy input by the winds is dominantly balanced by APE removal by the GM parameterization, which is ultimately dissipated at the subgrid scale (cf. Figure 1). Bottom friction acting on the resolved flow (the dominant energy sink in the

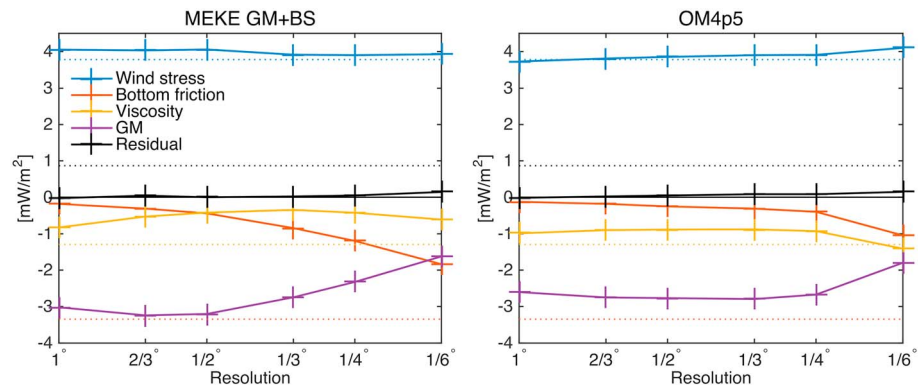


**Figure 11.** Energy budget of the resolved flow, as a function of resolution, for the simulations with the new MEKE GM+BS parameterization (left) and the parameterization used in OM4p5 (right). Shown are the kinetic energy (KE) input by the wind stress (blue), KE dissipation by bottom friction (red), the net KE dissipation by viscous terms (including both biharmonic viscosity and negative Laplacian backscatter; yellow), potential energy dissipation by the GM parameterization (purple), as well as the residual (black). The dotted horizontal lines indicate the corresponding values in the fine-resolution reference simulation. The significant residual in the energy budget of the fine-resolution reference simulation indicates a spurious numerical energy source, which appears to arise primarily from the discretization of the momentum equation (see section 3). Notice that the model diagnostics provide only the net energy tendency associated with vertical momentum transfer. The energy input by wind stress and dissipation by bottom friction are estimated by integrating this energy tendency over outcropping and incropping layers, respectively.

fine-resolution reference simulation) plays a negligible role. As the resolution increases, the role of the GM parameterization is reduced, while resolved bottom friction becomes increasingly important. The net viscous KE dissipation, which includes both the dissipation by the biharmonic viscosity and the backscatter, is relatively small at all resolutions, implying a weak net KE cascade. The energy fluxes at coarse resolution are similar to those obtained with the traditional GM parameterizations (without backscatter) such as in the OM4p5 configuration. Unlike with the MEKE GM+BS parameterization, the energy budget with the OM4p5 parameterization, however, remains essentially unchanged until the resolution is increased to  $(1/6)^\circ$ , at which point the GM parameterization starts to be turned off. Due to the lack of energy backscatter, viscous energy dissipation is also larger with the OM4p5 configuration, particularly at higher resolutions. This is despite the fact that the simulations using the OM4p5 parameterization configuration have a substantially weaker and smoother resolved flow. Notice that viscous dissipation is also a nonnegligible term in the  $(1/16)^\circ$  resolution reference simulation. We do not know whether this dissipation is physical or primarily the result of still insufficient resolution.

## 5. Summary and Discussion

A new parameterization for subgrid mesoscale eddies is introduced, which aims to allow for a seamless connection between non-eddy and eddy-resolving resolution regimes. The formulation is motivated by the theory of geostrophic turbulence, which suggests that mesoscale subgrid eddy closures should account for the possibility of KE backscatter to the resolved flow. This pathway is likely to be of particular importance at eddy-permitting resolutions, where traditional viscous closures extract large amounts of KE, while the KE cascade is in reality likely to be weak and potentially inverse (i.e., directed toward larger scales; e.g., Charney, 1971; Larichev & Held, 1995; Rhines, 1979; Salmon, 1980). The new parameterization uses an explicit subgrid energy budget and allows for APE and KE transfer to the subgrid scales via GM and hyperviscosity, as well as KE backscatter to the resolved flow via a negative viscosity.

The parameterization has been implemented in GFDL's MOM6 ocean model and tested in the Neverworld configuration, which represents an idealized model of the Southern Hemisphere. Simulation results at coarse resolution are evaluated by comparison against a high-resolution reference simulation, considering a number of objective measures of both eddy and mean flow properties.

The new parameterization leads to significant improvements compared to various formulations of the GM parameterization, particularly at resolutions of around  $(1/2)^\circ$  and finer. The backscatter term allows for a more energetic resolved flow with more realistic internal variability, as compared to simulations using a

GM parameterization without energy backscatter. Resolved KE levels and variability are of roughly similar magnitude as found in simulations that do not employ any GM parameterization. Simulations without GM, however, poorly represent the mean flow at resolution coarser than  $(1/4)^\circ$ . The new parameterization, in contrast, allows for a relatively faithful representation of the mean flow throughout the full range of considered resolutions.

Perhaps most importantly, the proposed formulation allows for a smooth connection between non-eddy and eddy-resolving resolution regimes. Previous work has argued that mesoscale eddy effects should be either fully or not at all parameterized using the GM parameterization, as any gradual reduction of the GM coefficient with increasing resolution will lead to a damping of the otherwise resolvable eddies, while contributing too little to the extraction of APE from the large-scale mean flow (Hallberg, 2013). The results of Hallberg (2013) are consistent with our argument that existing GM and eddy viscosity parameterizations are too dissipative at eddy-permitting resolutions, as they are missing KE backscatter to the resolved flow. Including a KE backscatter term allows us to parameterize the effects of the unresolved motions while keeping the resolved flow energized. A parameterization that applies across a wide range of resolutions, from non-eddy to eddy resolving, is crucial for global ocean and climate models, which may be eddy resolving or permitting in some regions but remain non-eddy in others (Hallberg, 2013). The resolution awareness also facilitates application in models that use nesting or variable meshes to locally refine the resolution (e.g., Biastoch et al., 2018; Ringler et al., 2013; Sein et al., 2016).

Our results also point to a number of issues that deserve further attention. One important topic is the formulation of subgrid KE dissipation, which ties in with the broader question of how mesoscale eddy energy is dissipated in the ocean (e.g., Wunsch & Ferrari, 2004). The present implementation assumes that subgrid KE dissipation is dominated by bottom friction and that the subgrid KE at the bottom is similar to the vertical average. However, an analysis of the fine-resolution reference simulation suggests that KE dissipation by viscosity is significant even at  $(1/16)^\circ$  resolution and that at least the total bottom KE is weaker than the vertical average (not shown). The pathways to dissipation in the real ocean may differ again, suggesting that the topic may need to be revisited in the context of a more realistic model. A somewhat related question remains with regard to the formulation of the backscatter parameterization at fine resolution. In the current implementation, the negative viscosity is formulated identically to the GM parameterization, which implies a relatively rapid falloff once the resolution exceeds the deformation radius. Whether a rapid reduction of backscatter at fine resolution is desirable likely depends on whether grid-scale motions are expected to remain balanced. A Rossby-number based modification of the backscatter parameterization was introduced by Klöwer et al. (2018) and may better be able to address the conditions under which backscatter should be suppressed.

A number of studies have highlighted the importance of along-isopycnal tracer fluxes in governing ocean ventilation (e.g., Burke et al., 2015; Gnanadesikan et al., 2015; Robbins et al., 2000)—a subject that has not been addressed by this study, which instead focuses on the parameterization of buoyancy and momentum fluxes. While a quantitative assessment of parameterized subgrid-scale eddy tracer fluxes will need to be left for future work, theoretical considerations suggest that the closure could be applied to eddy tracer fluxes with an along-isopycnal diffusivity similar to  $K_{GM}$ , albeit without the additional tapering of the diffusivity for  $\Delta k_d \lesssim 1$ . The tapering via  $R(\Delta k_d)$  aims to account for the lack of an APE cascade below the deformation radius and hence does not apply to passive tracers, whose variance undergoes a forward cascade to the microscale.

Bachman (2019) independently developed a related approach to couple the GM parameterization with KE backscatter. As in the parameterization proposed here, the motivation is that the APE dissipation implied by the GM parameterization causes spurious energy dissipation unless we account for the return of KE to the resolved flow. Unlike the approach discussed here, the formulation of Bachman (2019) does not include an explicit subgrid KE budget but instead computes the magnitude of energy backscatter such as to instantaneously balance the energy dissipation by the GM parameterization. The GM parameterization and viscous dissipation are formulated using the QG Leith parameterization of Bachman et al. (2017), which includes a Laplacian rather than biharmonic viscosity, and the backscatter is formulated as a

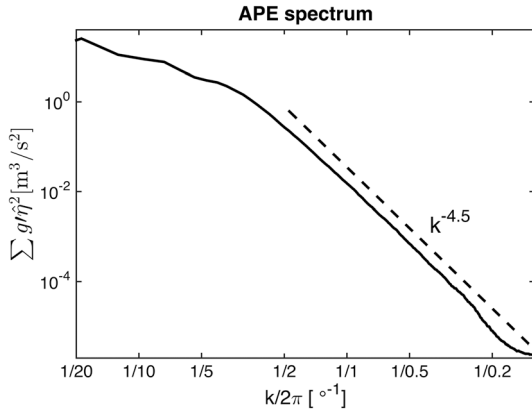


**Figure A1.** Zonal spectrum of available potential energy (APE), computed as  $\langle \sum_n g'_n |\hat{\eta}_n|^2 \rangle$  where  $\hat{\eta}_n(k, y)$  is the zonal Fourier transform of the  $n$ th interface height,  $g'_n$  is the corresponding reduced gravity, and the sum extends over all layer interfaces. The overbar represents time-averaging over the last 10 years of the simulation, and the angle brackets represent meridional averages over the two basin regions (defined as for the kinetic energy spectra in Figure 4). The dashed line indicates a slope of  $k^{-4.5}$ .

negative viscosity acting only on the barotropic flow component. A systematic analysis of the effects of these various differences is beyond the scope of this study but may provide a promising route toward a closure that combines successful aspects of both approaches.

The KE backscatter parameterizations developed here and by Bachman (2019) follow up on a number of related approaches investigated in recent years (Berloff, 2016; Grooms et al., 2015; Jansen & Held, 2014; Jansen et al., 2015; Mana & Zanna, 2014; Zanna et al., 2017), all of which highlight the importance to energize the resolved flow at eddy-permitting resolutions. Together, the promising results obtained by these studies raise hope that energetically consistent parameterizations that account for KE backscatter to the resolved flow can lead to significant improvements in global ocean simulations and allow us to effectively leverage the increasing resolution of climate models.

### Appendix A: Scaling Argument for the GM Coefficient for $\Delta^{-1} \gg k_d$

Most of the mesoscale energy in the ocean is in the barotropic and first baroclinic modes (Wunsch, 1997), which suggests that two-layer QG theory provides a reasonable starting point to understand the dominant

dynamics and energetics. We will here focus on the theoretical framework described by Larichev and Held (1995) and Held and Larichev (1996), which in turn builds on earlier work described by Rhines (1979) and Salmon (1980). According to that theory, APE (or more generally baroclinic mode energy, which for  $k < k_d$  is dominantly in the form of APE) cascades toward smaller scales for  $k < k_d$ , until the deformation radius is reached, where the APE is transferred into barotropic KE, which then cascades inversely toward larger scales. At  $k \gg k_d$  we instead expect only a cascade of enstrophy, with a  $k^{-3}$  KE spectrum. Moreover, the two layers become independent for  $k \gg k_d$ , leading to an equipartitioning of energy between the baroclinic and barotropic modes (as in fact predicted across all scales), and a ratio of EKE to APE proportional to  $k^2/k_d^2$ .

Noting that, for isotropic flow,  $|\hat{v}|^2 \propto \text{KE}(k)$ , where  $\hat{v}$  is the meridional velocity spectrum and  $|\hat{\eta}|^2 \propto \text{APE}(k)$ , where  $\hat{\eta}$  is the layer interface height spectrum, we may expect the eddy volume flux spectrum,  $\hat{v}\hat{\eta}^*$ , where  $(\ )^*$  denotes the complex conjugate, to be proportional to the square root of the product of the APE and KE spectra (see also Marshall et al., 2012). With  $\text{KE}(k) \propto k^{-3}$  and  $\text{APE}(k) \propto k^{-5}$ , this leads us to a flux spectrum proportional to  $k^{-4}$ . The total eddy volume flux accomplished by eddies smaller than some hypothetical Nyquist frequency  $k_N \propto \Delta^{-1}$  is hence expected to be proportional to  $k_N^{-3} \propto \Delta^3$ . We want to parameterize this volume flux using a GM closure where  $(v\eta)_{\text{SGS}} = -K_{\text{GM}} \nabla \eta$ , where  $(v\eta)_{\text{SGS}}$  represents the unresolved (subgrid-scale) flux and  $\eta$  the resolved interface height. Due to the steep APE spectrum for  $k > k_d$ ,  $\nabla \eta$  is expected to be approximately independent of resolution (once the deformation scale is resolved), and hence, we need  $K_{\text{GM}} \propto \Delta^3$ . Using the formulation of the GM coefficient in equation (2) and noting that the subgrid EKE itself is expected to be proportional to  $\Delta^2$  in the enstrophy inertial range, this requires  $R(\Delta/k_d) \propto (\Delta/k_d)$  for  $\Delta^{-1} \gg k_d$ .

The argument above is based on a two-layer model, which may not be adequate in the presence of higher vertical modes. If higher modes become increasingly important at smaller scales and lead to an equipartition of energy between APE and KE, we may expect a flatter APE spectrum, proportional to  $k^{-3}$ , which would lead us to estimate a GM coefficient proportional to  $\Delta^2$ , thus rendering the resolution function unnecessary. An estimate of the geostrophic APE spectrum in the high-resolution Neverworld simulations confirms a relatively steep slope of around  $k^{-4.5}$  (Figure A1), not too different from the prediction of two-layer QG theory, which supports the use of the resolution function.

### Appendix B: The OM4p5 Eddy Parameterization

The OM4p5 configuration uses an explicit subgrid energy budget, similar to equation (1), although without the viscous energy transfer terms, that is,  $e_{v_4} = e_{v_2} = 0$ . The GM parameterization is formulated as in equation (2), although the eddy energy  $e$  is replaced by an estimate of its barotropic component,  $e_t$ , which in

turn is computed following Jansen et al. (2015). Moreover, different formulations are used for the definition of the mixing length and resolution function. The mixing length is defined as

$$L_{\text{mix}} = (L_{\beta}^{-1} + L_{\text{LH}}^{-1})^{-1}, \quad (\text{B1})$$

where  $L_{\beta} = (2e_t)^{1/4}\beta^{-1/2}$  is the Rhines scale (unaffected by topography) and  $L_{\text{LH}} = 2e_t/[sN]$  a maximum mixing length implied by assuming a decorrelation timescale  $\tau_{\text{LH}} \sim [sN]^{-1}$  (see Jansen et al., 2015; Larichev & Held, 1995). The resolution function is defined (following Hallberg, 2013) as

$$R(\Delta k_d) = \mathcal{H}(\Delta k_d - 1), \quad (\text{B2})$$

where  $\mathcal{H}$  is the Heaviside step function. The vertical structure of the GM diffusivity is further modulated by multiplication with the vertical structure of the first equivalent barotropic mode, computed from the local stratification by solving for the first eigenmode with a no-slip bottom boundary condition (Hallberg, 1997).

Subgrid dissipation is computed as in equation (9) but with  $e$  replaced by an estimate of the energy near the bottom,  $e_b$ , computed following Jansen et al. (2015). We found that using the estimated barotropic and bottom eddy energies for the formulation of the GM coefficient and frictional dissipation, following Jansen et al. (2015), makes little difference and leads to no significant improvement once the overall magnitude of the GM parameter is retuned accordingly, which is why this formulation has not been adopted for the parameterization presented in section 2.

Unlike any of the other approaches discussed in this paper, the OM4p5 configuration also uses a positive (i.e., dissipative) Laplacian viscosity. The viscosity coefficient is computed as the sum of four parts: (1) a MEKE-based viscosity formulated similarly to the GM coefficient (albeit with a viscosity that is twice as large as the GM coefficient), (2) a Smagorinsky viscosity with  $C_{\text{smag},v_2} = 0.15$ , (3) a grid-scale-dependent background viscosity,  $\nu_{\Delta} = 0.01 \text{ m}^2/\text{s}\Delta$ , and (4) an additional latitudinally dependent background viscosity with a maximum value of  $2000 \text{ m}^2/\text{s}$  at the poles and decreasing equatorward as  $\sin^4(\phi)$ . The Laplacian viscosity is subject to the same resolution step function scaling as the GM coefficient; that is, the viscosity is turned off once the grid scale is finer than the deformation radius.

#### Acknowledgments

Computing resources for this study were provided by the University of Chicago Research Computing Center (RCC). Financial support was provided by the National Science Foundation through Awards 1536360 and 1536450. The MOM6 version used for this paper is available on GitHub (<https://github.com/MFJansen/MOM6>), and parameter files for the specific simulations are also available on GitHub ([https://github.com/MFJansen/MEKE\\_GM\\_BS\\_parameters](https://github.com/MFJansen/MEKE_GM_BS_parameters)). The documentation of MOM6 is available online (<https://mom6.readthedocs.io/en/dev-gfdl/>). We wish to thank Steve Griffies and John Dunne for comments on an earlier version of this manuscript. We also thank Ian Grooms and an anonymous reviewer for insightful comments, which helped to improve the manuscript.

#### References

- Arakawa, A., & Hsu, Y.-J. G. (1990). Energy conserving and potential-enstrophy dissipating schemes for the shallow water equations. *Monthly Weather Review*, *118*, 1960–1969.
- Arbic, B. K., Polzin, K. L., Scott, R. B., Richman, J. G., & Shriver, J. F. (2013). On eddy viscosity, energy cascades, and the horizontal resolution of gridded satellite altimeter products. *Journal of Physical Oceanography*, *43*, 283–300.
- Bachman, S. D. (2019). The GM+E closure: A framework for coupling backscatter with the Gent and McWilliams parameterization. *Ocean Modelling*, *136*, 85–106. <https://doi.org/10.1016/j.ocemod.2019.02.006>
- Bachman, S. D., Fox-Kemper, B., & Pearson, B. (2017). A scale-aware subgrid model for quasi-geostrophic turbulence. *Journal of Geophysical Research: Oceans*, *122*, 1529–1554. <https://doi.org/10.1002/2016JC012265>
- Berloff, P. (2016). Dynamically consistent parameterization of mesoscale eddies. Part II: Eddy fluxes and diffusivity from transient impulses. *Fluids*, *1*(3), 22.
- Biastoch, A., Sein, D., Durgadoo, J. V., Wang, Q., & Danilov, S. (2018). Simulating the Agulhas system in global ocean models—nesting vs. multi-resolution unstructured meshes. *Ocean Modelling*, *121*, 117–131.
- Burke, A., Stewart, A. L., Adkins, J. F., Ferrari, R., Jansen, M. F., & Thompson, A. F. (2015). The glacial mid-depth radiocarbon bulge and its implications for the overturning circulation. *Paleoceanography and Paleoclimatology*, *30*, 1021–1039.
- Busecke, J., Gordon, A. L., Li, Z., Bingham, F. M., & Font, J. (2014). Subtropical surface layer salinity budget and the role of mesoscale turbulence. *Journal of Geophysical Research: Oceans*, *119*, 4124–4140. <https://doi.org/10.1002/2013JC009715>
- Cessi, P. (2008). An energy-constrained parameterization of eddy buoyancy flux. *Journal of Physical Oceanography*, *38*, 1807–1819.
- Charney, J. G. (1971). Geostrophic turbulence. *Journal of the Atmospheric Sciences*, *28*, 1087–1094.
- Chen, R., Flierl, G. R., & Wunsch, C. (2014). A description of local and nonlocal eddy–mean flow interaction in a global eddy-permitting state estimate. *Journal of Physical Oceanography*, *44*(9), 2336–2352.
- Chen, R., Thompson, A. F., & Flierl, G. R. (2016). Time-dependent eddy-mean energy diagrams and their application to the ocean. *Journal of Physical Oceanography*, *46*(9), 2827–2850.
- Eden, C., & Greatbatch, R. J. (2008). Towards a mesoscale eddy closure. *Ocean Modelling*, *20*(3), 223–239.
- Ferrari, R., & Wunsch, C. (2009). Ocean circulation kinetic energy—Reservoirs, sources and sinks. *Annual Review of Fluid Mechanics*, *41*, 253–282.
- Flierl, G. R. (1978). Models of vertical structure and the calibration of two-layer models. *Dynamics of Atmospheres and Oceans*, *2*, 341–381.
- Fox-Kemper, B., & Menemenlis, D. (2008). Can large eddy simulation techniques improve mesoscale rich ocean models? In M. W. Hecht, & H. Hasumi (Eds.), *Ocean modeling in an eddy regime* (vol. 177, pp. 319–337). Washington, D.C.: American Geophysical Union. <https://doi.org/10.1029/177GM19>
- Gent, P. R., & McWilliams, J. C. (1990). Isopycnal mixing in ocean circulation models. *Journal of Physical Oceanography*, *20*, 150–155.
- Gill, A. E., Green, J. S. A., & Simmons, A. J. (1974). Energy partition in the large-scale ocean circulation and the production of mid-ocean eddies. *Deep Sea Research*, *21*(7), 499–528.

- Gnanadesikan, A., Pradal, M.-A., & Abernathy, R. (2015). Isopycnal mixing by mesoscale eddies significantly impacts oceanic anthropogenic carbon uptake. *Geophysical Research Letters*, *42*, 4249–4255. <https://doi.org/10.1002/2015GL064100>
- Green, J. S. A. (1970). Transfer properties of the large-scale eddies and the general circulation of the atmosphere. *Quarterly Journal of the Royal Meteorological Society*, *96*, 157–185.
- Griffies, S. M., & Hallberg, R. (2000). Biharmonic friction with a Smagorinsky-like viscosity for use in large-scale eddy-permitting ocean models. *Monthly Weather Review*, *128*, 2935–2946.
- Griffies, S. M., Winton, M., Anderson, W. G., Benson, R., Delworth, T. L., Dufour, C. O., et al. (2015). Impacts on ocean heat from transient mesoscale eddies in a hierarchy of climate models. *Journal of Climate*, *28*(3), 952–977.
- Grooms, I. (2017). Simulations of eddy kinetic energy transport in barotropic turbulence. *Physical Review Fluids*, *2*(11), 113801.
- Grooms, I., Lee, Y., & Majda, A. J. (2015). Numerical schemes for stochastic backscatter in the inverse cascade of quasigeostrophic turbulence. *Multiscale Modeling & Simulation*, *13*(3), 1001–1021.
- Hallberg, R. (1997). Localized coupling between surface and bottom-intensified flow over topography. *Journal of Physical Oceanography*, *27*, 977–998.
- Hallberg, R. (2013). Using a resolution function to regulate parameterizations of oceanic mesoscale eddy effects. *Ocean Modelling*, *72*, 92–103.
- Hallberg, R., & Gnanadesikan, A. (2006). The role of eddies in determining the structure and response of the wind-driven southern hemisphere overturning: Results from the Modeling Eddies in the Southern Ocean (MESO) project. *Journal of Physical Oceanography*, *36*(12), 2232–2252.
- Held, I. M., & Larichev, V. D. (1996). A scaling theory for horizontally homogeneous baroclinically unstable flow on a beta plane. *Journal of the Atmospheric Sciences*, *53*(7), 946–952.
- Jansen, M. F., Adcroft, A. J., Hallberg, R., & Held, I. M. (2015). Parameterization of eddy fluxes based on a mesoscale energy budget. *Ocean Modelling*, *92*, 28–41.
- Jansen, M. F., & Held, I. M. (2014). Parameterizing subgrid-scale eddy effects using energetically consistent backscatter. *Ocean Modelling*, *80*, 36–48.
- Jansen, M. F., Held, I. M., Adcroft, A., & Hallberg, R. (2015). Energy budget-based backscatter in an eddy permitting primitive equation model. *Ocean Modelling*, *94*, 15–26.
- Johnson, G. C., & Bryden, H. L. (1989). On the size of the Antarctic Circumpolar Current. *Deep Sea Research Part A. Oceanographic Research Papers*, *36*(1), 39–53.
- Juricke, S., Danilov, S., Kutsenko, A., & Oliver, M. (2019). Ocean kinetic energy backscatter parameterizations on unstructured grids: Impact on mesoscale turbulence in a channel. *Ocean Modelling*, *138*, 51–67. <https://doi.org/10.1016/j.ocemod.2019.03.009>
- Klöwer, M., Jansen, M. F., Claus, M., Greatbatch, R. J., & Thomsen, S. (2018). Energy budget-based backscatter in a shallow water model of a double gyre basin. *Ocean Modelling*, *132*, 1–11.
- Kuhlbrodt, T., Gregory, J., & Shaffrey, L. (2015). A process-based analysis of ocean heat uptake in an AOGCM with an eddy-permitting ocean component. *Climate Dynamics*, *45*(11–12), 3205–3226.
- Larichev, V. D., & Held, I. M. (1995). Eddy amplitudes and fluxes in a homogeneous model of fully developed baroclinic instability. *Journal of Physical Oceanography*, *25*, 2285–2297.
- Lorenz, E. N. (1955). Available potential energy and the maintenance of the general circulation. *Tellus*, *7*(2), 157–167.
- Mak, J., Maddison, J., Marshall, D., & Munday, D. R. (2018). Implementation of a geometrically informed and energetically constrained mesoscale eddy parameterization in an ocean circulation model. *Journal of Physical Oceanography*, *48*(10), 2363–2382.
- Mak, J., Marshall, D., Maddison, J., & Bachman, S. D. (2017). Emergent eddy saturation from an energy constrained eddy parameterisation. *Ocean Modelling*, *112*, 125–138.
- Mana, P. P., & Zanna, L. (2014). Toward a stochastic parameterization of ocean mesoscale eddies. *Ocean Modelling*, *79*, 1–20.
- Marshall, D. P., & Adcroft, A. J. (2010). Parameterization of ocean eddies: Potential vorticity mixing, energetics and Arnold's first stability theorem. *Ocean Modelling*, *32*(3–4), 188–204. The magic of modelling: A special volume commemorating the contributions of Peter D. Killworth – Part 2.
- Marshall, D. P., Maddison, J. R., & Berloff, P. S. (2012). A framework for parameterizing eddy potential vorticity fluxes. *Journal of Physical Oceanography*, *42*(4), 539–557.
- McWilliams, J. C. (2008). The nature and consequences of oceanic eddies. *Geophysical monograph series* (Vol. 177, pp. 5–15). Washington, D. C.: American Geophysical Union.
- Meijers, A. (2014). The Southern Ocean in the coupled model intercomparison project phase 5. *Philosophical Transactions of the Royal Society A: Mathematical, Physical and Engineering Sciences*, *372*(2019), 20130296.
- Menemenlis, D., Campin, J.-M., Heimbach, P., Hill, C., Lee, T., Nguyen, A., et al. (2008). ECCO2: High resolution global ocean and sea ice data synthesis. *Mercator Ocean Quarterly Newsletter*, *31*(October), 13–21.
- Rhines, P. B. (1979). Geostrophic turbulence. *Annual Review of Fluid Mechanics*, *11*, 401–441.
- Ringler, T., Petersen, M., Higdon, R. L., Jacobsen, D., Jones, P. W., & Maltrud, M. (2013). A multi-resolution approach to global ocean modeling. *Ocean Modelling*, *69*, 211–232.
- Robbins, P. E., Price, J. F., Owens, W. B., & Jenkins, W. J. (2000). The importance of lateral diffusion for the ventilation of the lower thermocline in the subtropical north atlantic. *Journal of Physical Oceanography*, *30*(1), 67–89.
- Roberts, M., & Marshall, D. (1998). Do we require adiabatic dissipation schemes in eddy-resolving ocean models? *Journal of Physical Oceanography*, *28*, 2050–2063.
- Sadourny, R. (1975). The dynamics of finite-difference models of the shallow-water equations. *Journal of the Atmospheric Sciences*, *32*, 680–689.
- Salmon, R. (1980). Baroclinic instability and geostrophic turbulence. *Geophysical & Astrophysical Fluid Dynamics*, *15*(1), 67–211.
- Scott, R. B., & Wang, F. (2005). Direct evidence of an oceanic inverse kinetic energy cascade from satellite altimetry. *Journal of Physical Oceanography*, *35*, 1650–1666.
- Sein, D. V., Danilov, S., Biastoch, A., Durgadoo, J. V., Sidorenko, D., Harig, S., & Wang, Q. (2016). Designing variable ocean model resolution based on the observed ocean variability. *Journal of Advances in Modeling Earth Systems*, *8*, 904–916. <https://doi.org/10.1002/2016MS000650>
- Sinha, B., & Richards, K. (1999). Jet structure and scaling in southern ocean models. *Journal of Physical Oceanography*, *29*(6), 1143–1155.
- Smagorinsky, J. (1963). General circulation experiments with the primitive equations. *Monthly Weather Review*, *91*, 99–164.
- Thompson, A. F. (2010). Jet formation and evolution in baroclinic turbulence with simple topography. *Journal of Physical Oceanography*, *40*(2), 257–278.

- Tulloch, R., Marshall, J., Hill, C., & Smith, K. S. (2011). Scales, growth rates and spectral fluxes of baroclinic instability in the ocean. *Journal of Physical Oceanography*, *41*, 1057–1076.
- Vallis, G. K. (2006). *Atmospheric and oceanic fluid dynamics* (pp. 745). Cambridge, UK: Cambridge University Press.
- Visbeck, M., Marshall, J., Haine, T., & Spall, M. (1997). Specification of eddy transfer coefficients in coarse-resolution ocean circulation models. *Journal of Physical Oceanography*, *27*, 381–402.
- von Storch, J.-S., Eden, C., Fast, I., Haak, H., Hernández-Deckers, D., Maier-Reimer, E., et al. (2012). An estimate of the Lorenz energy cycle for the world ocean based on the STORM/NCEP simulation. *Journal of Physical Oceanography*, *42*(12), 2185–2205.
- Waterman, S., Hogg, N. G., & Jayne, S. R. (2011). Eddy-mean flow interaction in the Kuroshio extension region. *Journal of Physical Oceanography*, *41*, 1182–1208.
- Wunsch, C. (1997). The vertical partition of oceanic horizontal kinetic energy. *Journal of Physical Oceanography*, *27*, 1770–1794.
- Wunsch, C., & Ferrari, R. (2004). Vertical mixing, energy, and the general circulation of the oceans. *Annual Review of Fluid Mechanics*, *36*, 281–314.
- Zanna, L., Mana, P. P., Anstey, J., David, T., & Bolton, T. (2017). Scale-aware deterministic and stochastic parametrizations of eddy-mean flow interaction. *Ocean Modelling*, *111*, 66–80.
- Zhai, X., Johnson, H. L., & Marshall, D. P. (2010). Significant sink of ocean-eddy energy near western boundaries. *Nature Geoscience*, *3*(9), 608–612.